

Influence of excitation energy on microscopic quantum pathways for ultrafast charge transfer in van der Waals heterostructures

Niklas Hofmann,¹ Johannes Gradl,¹ Leonard Weigl,¹
Stiven Forti,^{2,3} Camilla Coletti,^{2,3} and Isabella Gierz^{4,*}

¹*Department for Experimental and Applied Physics,
University of Regensburg, 93053 Regensburg, Germany*

²*Center for Nanotechnology Innovation@NEST,
Istituto Italiano di Tecnologia, Pisa, Italy*

³*Graphene Labs, Istituto Italiano di Tecnologia, Genova, Italy*

⁴*Department for Experimental and Applied Physics,
University of Regensburg, Regensburg, Germany*

(Dated: August 28, 2025)

Abstract

Efficient charge separation in van der Waals (vdW) heterostructures is crucial for optimizing light-harvesting and detection applications. However, precise control over the microscopic pathways governing ultrafast charge transfer remains an open challenge. These pathways are intrinsically linked to charge transfer states with strongly delocalized wave functions that appear at various momenta in the Brillouin zone. Here, we use time- and angle-resolved photoemission spectroscopy (trARPES) to investigate the possibility of steering carriers through specific charge transfer states in a prototypical WS₂-graphene heterostructure. By selectively exciting electron-hole pairs at the K-point and close to the Q-point of WS₂ with different pump photon energies, we find that charge separation is faster at higher excitation energies. We attribute this to distinct tunneling mechanisms dictated by the momentum where the initial excitation takes place. Our findings reveal that the microscopic pathways for ultrafast charge transfer in vdW heterostructures are highly sensitive to the excitation energy, an aspect that should be carefully considered when optimizing the performance of optoelectronic devices.

INTRODUCTION

The vast selection of 2D materials available today, such as graphene and monolayer transition metal dichalcogenides, enables the design of novel heterostructures with tailored properties [1–3]. Efficient absorption of visible light followed by ultrafast charge separation [4–10] is a key feature of these heterostructures, offering great potential for applications in light harvesting and detection. The driving force behind ultrafast charge separation is the band alignment, where photoexcited electrons and holes rapidly relax to the conduction band minimum and valence band maximum in separate layers. Charge transfer states, formed by hybridization between the vdW-coupled layers, create delocalized wave functions that serve as ultrafast tunnelling channels [11–13]. These states occur at various momenta in the Brillouin zone but do not contribute equally to charge separation. Based on existing models [11, 13–18], the efficiency of different tunnelling channels depends on the orbital composition of charge transfer states, their momentum-space distribution, and tunnelling barriers that photoexcited carriers must overcome. Consequently, it should be possible to steer quantum pathways by selectively generating electron-hole pairs at specific momenta.

Here, we explore this concept in a prototypical vdW heterostructure consisting of mono-

layer WS₂ and graphene. We photoexcite the heterostructure with pump photon energies of $\hbar\omega = 2.0\text{ eV}$ and $\hbar\omega = 3.1\text{ eV}$ to excite electron-hole pairs at the K-point and in between the Γ - and Q-point (also referred to as Σ - or Λ -point) of WS₂, respectively, and probe the charge transfer dynamics directly in the band structure using time- and angle-resolved photoemission spectroscopy (trARPES) [19]. We find that charge separation is significantly faster for $\hbar\omega = 3.1\text{ eV}$, which we attribute to distinct quantum pathways for hole tunneling at different momenta in the Brillouin zone. Our findings introduce new possibilities for optimizing charge separation in vdW heterostructures, paving the way for more efficient light-harvesting and detection technologies.

METHODS

Sample growth: Pretreated 4H-SiC substrates were H-etched to remove scratches and graphitized in Ar atmosphere. The resulting carbon monolayer with $(6\sqrt{3} \times 6\sqrt{3})\text{ R}30^\circ$ structure was decoupled from the SiC substrate by H-intercalation, yielding quasi-freestanding monolayer graphene [20]. WS₂ was then grown by chemical vapour deposition (CVD) from solid WO₃ and S precursors [21, 22]. Both graphene and WS₂ growth were monitored using Raman spectroscopy, atomic force microscopy and secondary electron microscopy. WS₂ was found to grow in the shape of triangular islands with side lengths in the range of 300–700 nm with twist angles of either 0° or 30° with respect to the graphene layer [13].

trARPES: The setup was based on a Ti:Sa amplifier (Astrella, Coherent) with 1 kHz repetition rate, 35 fs pulse duration, 1.55 eV photon energy, and 7 mJ output power. Of this, 2 mJ were frequency-doubled and used to drive high harmonics generation (HHG) in an Argon gas jet. The 7th harmonic at 21.7 eV was isolated using a grating monochromator and focused onto the sample with a beam diameter of 250 μm . A small part of the 2 mJ output was frequency doubled to generate pump pulses with a photon energy of 3.1 eV with a fluence of 0.4 mJ/cm² at the focus. The remaining 5 mJ seeded an optical parametric amplifier (Topas Twins, Light Conversion). One of the signal beams was frequency doubled to generate pump pulses with a photon energy of 2.0 eV with a fluence of 1.7 mJ/cm² at the focus. The photoemitted electrons were detected with a hemispherical analyzer (Phoibos 100, SPECS) to obtain snapshots of the occupied band structure along the ΓK direction of graphene. The temporal and energy resolutions were $\approx 200\text{ meV}$ and $\approx 160\text{ fs}$, respectively.

RESULTS

Figure 1a shows an ARPES image of the WS₂-graphene heterostructure at negative pump-probe delay before the arrival of the pump pulse. The dotted, dashed, and continuous lines indicate the theoretical band structures of WS₂ islands with a twist angle of 0°, WS₂ islands with a twist angle of 30° [23] and graphene [24], respectively. The bands are shifted in energy to fit the experimentally observed band alignment and doping level. Orange and blue arrows mark the electronic transitions excited at $\hbar\omega = 2.0$ eV and $\hbar\omega = 3.1$ eV, respectively, in WS₂. Here, we will only consider WS₂ islands with 0° twist angle. The influence of the twist angle on ultrafast charge separation will be investigated in a separate work.

Figure 1b depicts the pump-induced changes of the photocurrent in Fig. 1a 240 fs after photoexcitation at $\hbar\omega = 2.0$ eV with a fluence of $F = 1.7$ mJ/cm². Brown and blue colors indicate a gain and loss of photoelectrons, respectively, with respect to negative pump-probe delay. Figure 1c is the same as Fig. 1b but for photoexcitation at $\hbar\omega = 3.1$ eV with a fluence of $F = 0.4$ mJ/cm² and 310 fs after photoexcitation. For both excitation energies we observe gain in the conduction band (CB) of WS₂, gain (loss) above (below) the equilibrium Fermi level in graphene, and a complex gain-loss signal in the WS₂ valence band (VB) with contributions from band shifts and broadening as previously discussed in [13, 18].

To gain access to the transient carrier population of different areas in the band structure, we integrate the photocurrent over the areas marked by the colored boxes in Figs. 1b and c. The corresponding pump-probe traces are shown in Fig. 2 together with single-exponential fits yielding the decay times τ . Dashed vertical lines in Fig. 2 indicate the pump-probe delay t_{\max} where the respective pump-probe trace reaches its maximum. The fit results are summarized in Table I. The charge carrier dynamics inside the Dirac cone (Fig. 2a) are found to be quite similar for $\hbar\omega = 2.0$ eV and $\hbar\omega = 3.1$ eV, respectively, considering that the pump pulses (grey-shaded areas in Fig. 2) were slightly longer for $\hbar\omega = 3.1$ eV than for $\hbar\omega = 2.0$ eV. The population dynamics of the WS₂ bands, however, show important differences when comparing the two excitation energies. We find that the gain above the equilibrium position of the WS₂ VB (Fig. 2b) reaches its maximum ≈ 250 fs later for $\hbar\omega = 2.0$ eV than for $\hbar\omega = 3.1$ eV. Further, for $\hbar\omega = 2.0$ eV the pump-probe signal of the WS₂ CB at K is much bigger than close to Q, indicating that the photoexcited electrons are mainly confined to the K valley (Fig. 3b1). For $\hbar\omega = 3.1$ eV, however, we find that the

population of the WS₂ CB at K is smaller than the one close to Q and reaches its maximum ≈ 130 fs later (Fig. 3b2).

To gain direct access to the timescales for ultrafast charge separation, we extract the related charging-induced band shifts of the WS₂ VB and CB as follows [13, 18]. First, we extract energy distribution curves (EDCs) at $k = 1.2 \text{ \AA}^{-1}$ from the trAPRES snapshots in Fig. 1 that we fit with an appropriate number of Gaussian peaks to obtain the transient binding energies shown in Fig. 3a. Next, we subtract the transient position of the WS₂ VB from the transient position of the WS₂ CB yielding the transient band gap E_{gap} shown in Fig. 3b. Finally, assuming that the band gap changes symmetrically around its center, we add (subtract) $E_{\text{gap}}/2$ to (from) the transient position of the WS₂ VB (CB) to obtain the shifts $\Delta E_{\text{charge}}^{\text{WS}_2}$ in Fig. 3c that we previously attributed to a transient charging of the WS₂ layer with excess electrons [13, 18]. The corresponding charging shift of the graphene layer in Fig. 3d is obtained by extracting momentum distribution curves (MDCs) in the energy range between 0.2 eV and 1.0 eV that we fit with a Lorentzian. The resulting peak positions are then multiplied with the slope of the Dirac cone to yield the data points in Fig. 3d. All orange and blue curves in Fig. 3 are single-exponential fits, the fit parameters of which are summarized in Table II. Vertical dashed orange and blue lines indicate the positions t_{max} , where the respective pump-probe signals reach their maximum. Note that the fit for the transient band gap in Fig. 3b is sensitive to the value assumed for the equilibrium gap size (we assumed 2.08 eV) which also affects $\Delta E_{\text{charge}}^{\text{WS}_2}$ in Fig. 3c. We would like to stress, though, that varying the equilibrium gap size by a reasonable amount has only a minor influence on the data points in Fig. 3c. Considering this, the behavior of the transient WS₂ band gap at $k = 1.2 \text{ \AA}^{-1}$ is very similar for $\hbar\omega = 2.0$ eV and $\hbar\omega = 3.1$ eV. In contrast to this, both the WS₂ and the graphene charging shifts are found to depend on the pump photon energy. We find that both charging shifts reach their maximum 160 – 340 fs later for $\hbar\omega = 2.0$ eV than for $\hbar\omega = 3.1$ eV.

DISCUSSION

The results obtained for $\hbar\omega = 2.0$ eV are in good agreement with previous trARPES results [13, 18, 25] making their interpretation straight forward. The asymmetric population dynamics of the Dirac cone (Fig. 2a1), the gain above the equilibrium position of the

WS₂ VB (Fig. 2b1) and the charging shifts in Figs. 3c and d provide direct evidence of ultrafast charge separation in the WS₂-graphene heterostructure, where hole transfer from WS₂ to graphene is much faster than electron transfer. The transient reduction of the band gap in Fig. 3b has been previously attributed to screening of the Coulomb interaction by photoinduced free carriers [19, 26–31].

The observed differences between excitation at $\hbar\omega = 2.0$ eV and $\hbar\omega = 3.1$ eV, however, deserve further discussion. We start with the observation that, for $\hbar\omega = 3.1$ eV, the population dynamics in the WS₂ CB in Fig. 2c2 are different at K and close to Q. The 3.1 eV pump pulse directly populates states close to the Q valley (see Fig. 1a). These carriers are then observed to scatter to the K valley within ≈ 130 fs (see Fig. 2c2) in good agreement with previously reported intervalley scattering times for WS₂ and similar TMDCs [32–36].

Next, we focus on the observation that the gain above the equilibrium position of the WS₂ VB (Fig. 2b) and the charging shifts in Fig. 3c and d are found to reach their extrema at earlier time delays for $\hbar\omega = 3.1$ eV than for $\hbar\omega = 2.0$ eV. This indicates that hole transfer is faster for $\hbar\omega = 3.1$ eV than for $\hbar\omega = 2.0$ eV. From [18] it is known that the rates for charge transfer from WS₂ to graphene increase with increasing electronic temperature as it becomes easier for the photoexcited carriers to overcome the energy barriers to possible charge transfer states. The transient electronic temperatures for the WS₂ layer are difficult to determine due to the small population of the WS₂ CB and the limited signal-to-noise ratio. The transient electronic temperature of the carriers inside the Dirac cone of graphene, however, can be extracted by fitting its transient population with a Fermi-Dirac distribution. The resulting electronic temperature is displayed in Fig. 4. We find that, despite differences in excitation energy and pump fluence, the transient electronic temperatures for $\hbar\omega = 2.0$ eV and $\hbar\omega = 3.1$ eV are very similar. Therefore, we conclude that differences in electronic temperature cannot account for the observation that hole transfer is faster for $\hbar\omega = 3.1$ eV.

Instead, we propose that the different hole transfer rates for $\hbar\omega = 2.0$ eV and $\hbar\omega = 3.1$ eV can be attributed to different tunneling pathways via different charge transfer states in the WS₂ VB. These charge transfer states have been previously identified using density functional theory calculations [13]. For convenience, we sketch the relevant part of the band structure of the WS₂-graphene heterostructure in Fig. 5. Charge transfer states, where the WS₂ and graphene bands hybridize, are shown in red. For $\hbar\omega = 2.0$ eV, photoexcitation occurs at the K valley of WS₂. The previously proposed scattering processes resulting in

ultrafast charge transfer to the graphene layer are indicated by orange arrows [13, 18]. For $\hbar\omega = 2.0$ eV, hole transfer is believed to occur via the charge transfer state located at $k > K$ in the WS₂ VB. Electrons likely transfer into the graphene layer via the charge transfer state located at $Q < k < K$ in the CB. For 3.1 eV excitation, electron-hole pairs are initially generated at momenta between Γ and Q. We propose that, on their way towards the VB maximum at K, these holes pass by the charge transfer state at $Q < k < K$ in the VB where they efficiently transfer into the graphene layer (blue arrows in Fig. 5). The reason why hole transfer at $Q < k < K$ is faster than at $k > K$ is that the size of the avoided crossing between WS₂ VB and graphene Dirac cone is bigger (and therefore hybridization is stronger) at $Q < k < K$ than at $k > K$ [13]. The charge transfer state for electrons inside the WS₂ CB is likely the same for $\hbar\omega = 2.0$ eV and $\hbar\omega = 3.1$ eV consistent with similar population lifetimes in Table I as well as similar decay times for the charging shifts in Table II.

SUMMARY AND OUTLOOK

In summary, we used trARPES of a WS₂-graphene heterostructure to show that electron-hole pairs positioned at different momenta in the Brillouin zone of WS₂ choose different quantum pathways to transfer into the vdW-coupled graphene layer. These results show that charge separation across vdW interfaces can be controlled via the incident pump photon energy, opening up new strategies to optimize the performance of vdW heterostructures for future applications in light harvesting and detection.

ACKNOWLEDGMENTS

This work received funding from the European Union’s Horizon 2020 research and innovation program under Grant Agreement No. 851280-ERC-2019-STG (DANCE) and No. 101130384 (QUONDENSATE), from the German Research Foundation (DFG) via the Collaborative Research Centre 1277 (Project No. 314695032) and the Research Unit 5242 (Project No. 449119662), as well as from the German Federal Ministry of Education and Research (BMBF) (Project No. 05K2022).

* isabella.gierz@ur.de

- [1] A. K. Geim and I. V. Grigorieva, Van der Waals heterostructures, *Nature* **499**, 419 (2013), arXiv:1307.6718.
- [2] K. S. Novoselov, A. Mishchenko, A. Carvalho, and A. H. Castro Neto, 2D materials and van der Waals heterostructures, *Science* **353**, 10.1126/science.aac9439 (2016).
- [3] C. Jin, E. Y. Ma, O. Karni, E. C. Regan, F. Wang, and T. F. Heinz, Ultrafast dynamics in van der Waals heterostructures, *Nature Nanotechnology* **13**, 994 (2018).
- [4] J. He, N. Kumar, M. Z. Bellus, H. Y. Chiu, D. He, Y. Wang, and H. Zhao, Electron transfer and coupling in graphene-tungsten disulfide van der Waals heterostructures, *Nature Communications* **5**, 10.1038/ncomms6622 (2014).
- [5] M. Massicotte, P. Schmidt, F. Violla, K. G. Schädler, A. Reserbat-Plantey, K. Watanabe, T. Taniguchi, K. J. Tielrooij, and F. H. Koppens, Picosecond photoresponse in van der Waals heterostructures, *Nature Nanotechnology* **11**, 42 (2016), arXiv:1507.06251.
- [6] J. He, D. He, Y. Wang, and H. Zhao, Probing effect of electric field on photocarrier transfer in graphene-WS₂ van der Waals heterostructures, *Optics Express* **25**, 1949 (2017).
- [7] Z. Ji, H. Hong, J. Zhang, Q. Zhang, W. Huang, T. Cao, R. Qiao, C. Liu, J. Liang, C. Jin, L. Jiao, K. Shi, S. Meng, and K. Liu, Robust Stacking-Independent Ultrafast Charge Transfer in MoS₂/WS₂ Bilayers, *ACS Nano* **11**, 12020 (2017).
- [8] Z. Song, H. Zhu, W. Shi, D. Sun, and S. Ruan, Ultrafast charge transfer in graphene-WS₂ Van der Waals heterostructures, *Optik* **174**, 62 (2018).
- [9] L. Yuan, T. F. Chung, A. Kuc, Y. Wan, Y. Xu, Y. P. Chen, T. Heine, and L. Huang, Photocarrier generation from interlayer charge-transfer transitions in WS₂-graphene heterostructures, *Science Advances* **4**, 1 (2018).
- [10] S. Fu, I. du Fossé, X. Jia, J. Xu, X. Yu, H. Zhang, W. Zheng, S. Krasel, Z. Chen, Z. M. Wang, K. J. Tielrooij, M. Bonn, A. J. Houtepen, and H. I. Wang, Long-lived charge separation following pump-wavelength-dependent ultrafast charge transfer in graphene/WS₂ heterostructures, *Science Advances* **7**, 1 (2021), arXiv:2007.08932.
- [11] Q. Zheng, W. A. Saidi, Y. Xie, Z. Lan, O. V. Prezhdo, H. Petek, and J. Zhao, Phonon-Assisted Ultrafast Charge Transfer at van der Waals Heterostructure Interface, *Nano Letters* **17**, 6435

- (2017).
- [12] J. Liu, X. Zhang, and G. Lu, Auger Processes and Excited State Dynamics in WS₂/Graphene Heterostructures: A First-Principles Perspective, *Journal of Physical Chemistry Letters* **13**, 7371 (2022).
 - [13] N. Hofmann, L. Weigl, J. Gradl, N. Mishra, G. Orlandini, S. Forti, C. Coletti, S. Latini, L. Xian, A. Rubio, D. Perez Paredes, R. Perea Causin, S. Brem, E. Malic, and I. Gierz, Link between interlayer hybridization and ultrafast charge transfer in WS₂-graphene heterostructures, *2D Materials* **10**, 035025 (2023).
 - [14] H. Wang, J. Bang, Y. Sun, L. Liang, D. West, V. Meunier, and S. Zhang, The role of collective motion in the ultrafast charge transfer in van der Waals heterostructures, *Nature Communications* **7**, 11504 (2016).
 - [15] R. Long and O. V. Prezhdo, Quantum Coherence Facilitates Efficient Charge Separation at a MoS₂/MoSe₂ van der Waals Junction, *Nano Letters* **16**, 1996 (2016).
 - [16] L. Li, R. Long, and O. V. Prezhdo, Charge Separation and Recombination in Two-Dimensional MoS₂/WS₂: Time-Domain ab Initio Modeling, *Chemistry of Materials* **29**, 2466 (2017).
 - [17] Y. Liu, J. Zhang, S. Meng, C. Yam, and T. Frauenheim, Electric Field Tunable Ultrafast Interlayer Charge Transfer in Graphene/WS₂Heterostructure, *Nano Letters* **21**, 4403 (2021).
 - [18] R. Krause, S. Aeschlimann, M. Ch, M. Chavez-Cervantes, R. Perea-Causin, S. Brem, E. Malic, S. Forti, F. Fabbri, C. Coletti, and I. Gierz, Microscopic understanding of ultrafast charge transfer in van-der-Waals heterostructures, *Physical Review Letters* **127**, 276401 (2021), arXiv:2012.09268.
 - [19] N. Hofmann, A. Steinhoff, R. Krause, N. Mishra, G. Orlandini, S. Forti, C. Coletti, T. O. Wehling, and I. Gierz, k-Resolved Ultrafast Light-Induced Band Renormalization in Monolayer WS₂ on Graphene, *Nano Letters* **25**, 1214 (2025).
 - [20] C. Riedl, C. Coletti, T. Iwasaki, A. A. Zakharov, and U. Starke, Quasi-free-standing epitaxial graphene on SiC obtained by hydrogen intercalation, *Physical Review Letters* **103**, 1 (2009).
 - [21] A. Rossi, H. Büch, C. Di Rienzo, V. Miseikis, D. Convertino, A. Al-Temimy, V. Voliani, M. Gemmi, V. Piazza, and C. Coletti, Scalable synthesis of WS₂ on graphene and h-BN: An all-2D platform for light-matter transduction, *2D Materials* **3**, 10.1088/2053-1583/3/3/031013 (2016).

- [22] S. Forti, A. Rossi, H. Büch, T. Cavallucci, F. Bisio, A. Sala, T. O. Mentş, A. Locatelli, M. Magnozzi, M. Canepa, K. Müller, S. Link, U. Starke, V. Tozzini, and C. Coletti, Electronic properties of single-layer tungsten disulfide on epitaxial graphene on silicon carbide, *Nanoscale* **9**, 16412 (2017).
- [23] H. Zeng, G. B. Liu, J. Dai, Y. Yan, B. Zhu, R. He, L. Xie, S. Xu, X. Chen, W. Yao, and X. Cui, Optical signature of symmetry variations and spin-valley coupling in atomically thin tungsten dichalcogenides, *Scientific Reports* **3**, 1608 (2013), arXiv:1208.5864.
- [24] P. R. Wallace, The Band Theory of Graphite, *Doboku Gakkai Ronbunshuu A* **71**, 622 (1947).
- [25] S. Aeschlimann, A. Rossi, M. Chávez-Cervantes, R. Krause, B. Arnoldi, B. Stadtmüller, M. Aeschlimann, S. Forti, F. Fabbri, C. Coletti, and I. Gierz, Direct evidence for efficient ultrafast charge separation in epitaxial WS₂/graphene heterostructures, *Science Advances* **6**, 2 (2020), arXiv:1904.01379.
- [26] M. M. Ugeda, A. J. Bradley, S. F. Shi, F. H. Da Jornada, Y. Zhang, D. Y. Qiu, W. Ruan, S. K. Mo, Z. Hussain, Z. X. Shen, F. Wang, S. G. Louie, and M. F. Crommie, Giant bandgap renormalization and excitonic effects in a monolayer transition metal dichalcogenide semiconductor, *Nature Materials* **13**, 1091 (2014).
- [27] A. Chernikov, C. Ruppert, H. M. Hill, A. F. Rigosi, and T. F. Heinz, Population inversion and giant bandgap renormalization in atomically thin WS₂ layers, *Nature Photonics* **9**, 466 (2015).
- [28] S. Ulstrup, A. G. Čabo, J. A. Miwa, J. M. Riley, S. S. Grønberg, J. C. Johannsen, C. Cacho, O. Alexander, R. T. Chapman, E. Springate, M. Bianchi, M. Dendzik, J. V. Lauritsen, P. D. King, and P. Hofmann, Ultrafast Band Structure Control of a Two-Dimensional Heterostructure, *ACS Nano* **10**, 6315 (2016), arXiv:1606.03555.
- [29] E. A. Pogna, M. Marsili, D. De Fazio, S. Dal Conte, C. Manzoni, D. Sangalli, D. Yoon, A. Lombardo, A. C. Ferrari, A. Marini, G. Cerullo, and D. Prezzi, Photo-induced bandgap renormalization governs the ultrafast response of single-layer MoS₂, *ACS Nano* **10**, 1182 (2016).
- [30] P. D. Cunningham, A. T. Hanbicki, K. M. McCreary, and B. T. Jonker, Photoinduced Bandgap Renormalization and Exciton Binding Energy Reduction in WS₂, *ACS Nano* **11**, 12601 (2017).
- [31] Y. Lin, Y. H. Chan, W. Lee, L. S. Lu, Z. Li, W. H. Chang, C. K. Shih, R. A. Kaindl, S. G. Louie, and A. Lanzara, Exciton-driven renormalization of quasiparticle band structure in monolayer MoS₂, *Physical Review B* **106**, 1 (2022), arXiv:2205.05821.

- [32] R. Wallauer, J. Reimann, N. Armbrust, J. Gdde, and U. Hfer, Intervalley scattering in MoS₂ imaged by two-photon photoemission with a high-harmonic probe, *Applied Physics Letters* **109**, 10.1063/1.4965839 (2016), arXiv:1607.04999.
- [33] R. Bertoni, C. W. Nicholson, L. Waldecker, H. Hbener, C. Monney, U. De Giovannini, M. Puppini, M. Hoesch, E. Springate, R. T. Chapman, C. Cacho, M. Wolf, A. Rubio, and R. Ernstorfer, Generation and Evolution of Spin-, Valley-, and Layer-Polarized Excited Carriers in Inversion-Symmetric WSe₂, *Physical Review Letters* **117**, 1 (2016), arXiv:1606.03218.
- [34] S. Dong, M. Puppini, T. Pincelli, S. Beaulieu, D. Christiansen, H. Hbener, C. W. Nicholson, R. P. Xian, M. Dendzik, Y. Deng, Y. W. Windsor, M. Selig, E. Malic, A. Rubio, A. Knorr, M. Wolf, L. Rettig, and R. Ernstorfer, Direct measurement of key exciton properties: Energy, dynamics, and spatial distribution of the wave function, *Natural Sciences* **1**, 1 (2021), arXiv:2012.15328.
- [35] R. Wallauer, R. Perea-Causin, L. Mnster, S. Zajusch, S. Brem, J. Gdde, K. Tanimura, K. Q. Lin, R. Huber, E. Malic, and U. Hfer, Momentum-Resolved Observation of Exciton Formation Dynamics in Monolayer WS₂, *Nano Letters* **21**, 5867 (2021), arXiv:2012.11385.
- [36] J. P. Bange, P. Werner, D. Schmitt, W. Bennecke, G. Meneghini, A. A. AlMutairi, M. Merboldt, K. Watanabe, T. Taniguchi, S. Steil, D. Steil, R. T. Weitz, S. Hofmann, G. S. Jansen, S. Brem, E. Malic, M. Reutzler, and S. Mathias, Ultrafast dynamics of bright and dark excitons in monolayer WSe₂ and heterobilayer WSe₂/MoS₂, *2D Materials* **10**, 035039 (2023), arXiv:2305.02111.

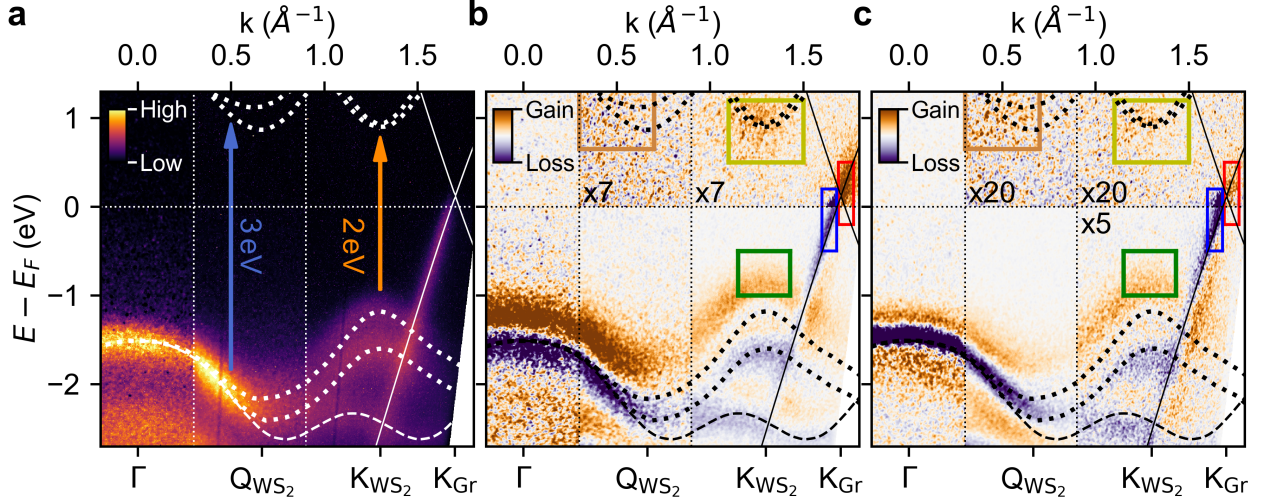


FIG. 1. **trARPES data of WS₂-graphene heterostructure.** **a)** ARPES snapshots for negative pump-probe delay taken along the ΓK direction of graphene. Orange and blue arrows indicate the two different excitation schemes for $\hbar\omega_{\text{pump}} = 2.0 \text{ meV}$ and $\hbar\omega_{\text{pump}} = 3.1 \text{ meV}$, respectively. Dotted, dashed and continuous lines represent the theoretical band structures for WS₂ with twist angles of 0° and 30° [23] and graphene [24], respectively. **b)** Pump-induced changes of the photocurrent in a) 240fs after excitation with $\hbar\omega_{\text{pump}} = 2.0 \text{ meV}$. **c)** Same as b) but 310fs after excitation with $\hbar\omega_{\text{pump}} = 3.1 \text{ meV}$. Colored boxes in b) and c) mark the regions of integration for the pump-probe traces displayed in Fig. 2.

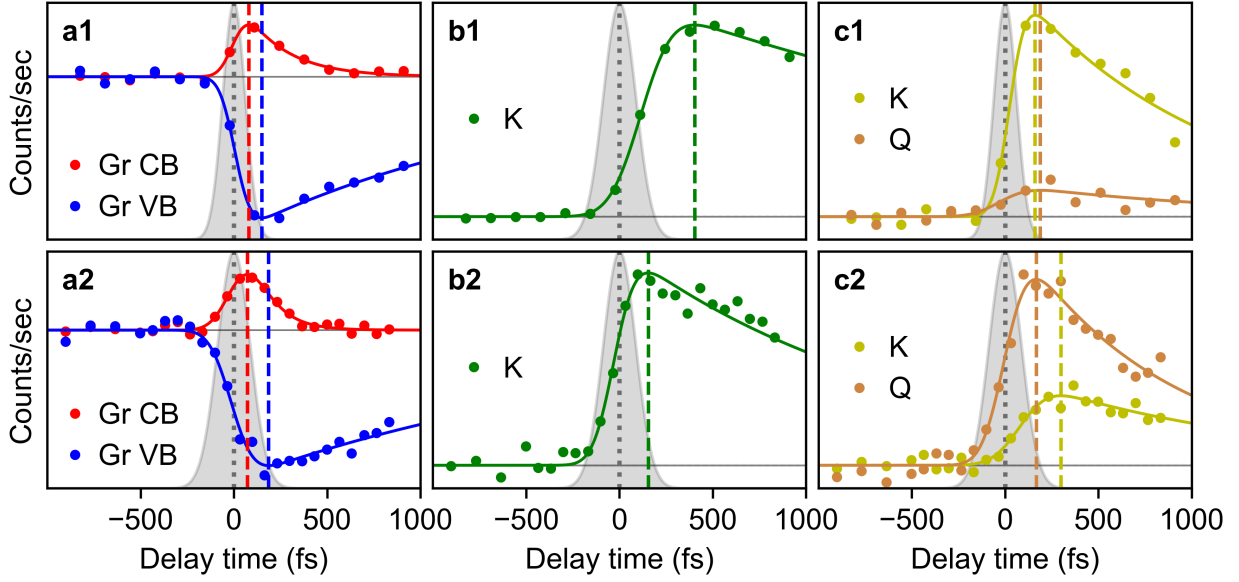


FIG. 2. **Population dynamics** obtained by integrating the counts over the areas marked by colored boxes in Figs. 1b and c. **a)** Gain (red) and loss (blue) inside the Dirac cone. **b)** Gain above the equilibrium position of the WS₂ VB at K. **c)** Population of the WS₂ CB at K (yellow) and close to Q (orange). Rows 1 and 2 present data for excitation at $\hbar\omega_{\text{pump}} = 2.0$ meV and $\hbar\omega_{\text{pump}} = 3.1$ meV, respectively. Continuous lines are single-exponential fits. Dashed colored lines indicate the pump-probe delay where the pump-probe traces reach their maximum. Grey-shaded areas indicate the temporal profile of the pump pulse.

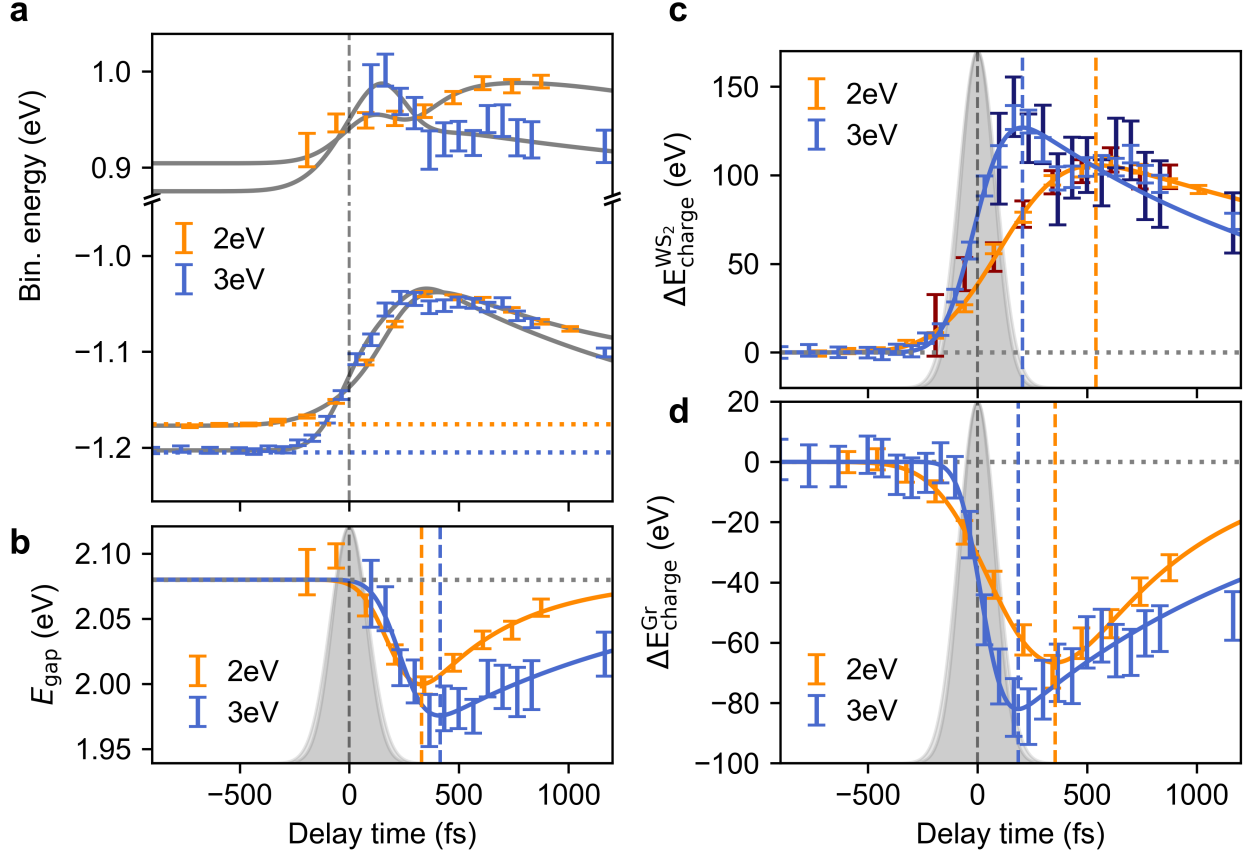


FIG. 3. **Transient band structure.** **a)** Transient band position of WS₂ CB (top) and VB (bottom). **b)** Transient band gap. **c)** Charging shifts of WS₂ VB and CB. **d)** Charging shift of Dirac cone. Data points for excitation at $\hbar\omega_{\text{pump}} = 2.0 \text{ meV}$ and $\hbar\omega_{\text{pump}} = 3.1 \text{ meV}$ are shown in orange and blue, respectively. Orange and blue curves are single-exponential fits. Grey curves in a) are guides to the eye calculated from the VB fit in a) and the gap fit in b) for the CB, and from the gap fit in b) and the charging shift fit in c) for the VB. Vertical colored dashed lines indicate the pump-probe delay where the pump-probe traces reach their maximum. Grey-shaded areas indicate the temporal profiles of the pump pulses.

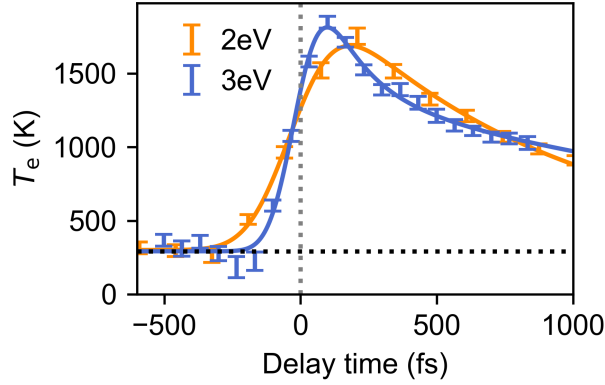


FIG. 4. **Transient electronic temperature inside the Dirac cone** obtained by fitting the transient carrier population of the Dirac cone with a Fermi-Dirac distribution. Data points for excitation at $\hbar\omega_{\text{pump}} = 2.0$ meV and $\hbar\omega_{\text{pump}} = 3.1$ meV are shown in orange and blue, respectively. Orange and blue lines are double-exponential fits that serve as guides to the eye.

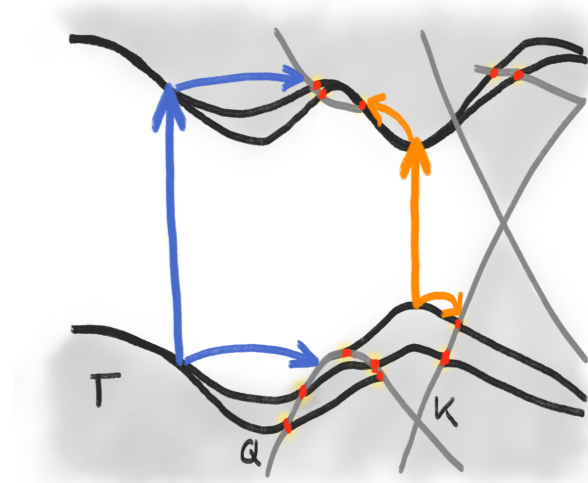


FIG. 5. **Schematic of quantum pathways for ultrafast charge transfer.** The band structure sketch is based on density functional theory calculations from [13]. The color code indicates whether the wave function is localized on the graphene layer (gray curves), the WS₂ layer (black curves) or delocalized over both layers (red dots). Blue (orange) arrows indicate direct optical transitions excited at $\hbar\omega_{\text{pump}} = 3.1$ meV ($\hbar\omega_{\text{pump}} = 2.0$ meV) and subsequent carrier relaxation via different charge transfer states.

	Red box	Blue box	Green box	Orange box	Yellow box
	Graphene gain	Graphene loss	Gain above equilibrium position of WS ₂ VB	Gain in WS ₂ CB at K	Gain in WS ₂ CB close to Q
$\tau_{2.0\text{eV}}$	230 ± 40 fs	1.7 ± 0.2 ps	3.2 ± 0.4 ps	1.0 ± 0.1 ps	1.3 ± 0.8 ps
$\tau_{3.1\text{eV}}$	120 ± 30 fs	2.2 ± 0.2 ps	1.5 ± 0.1 ps	0.8 ± 0.1 ps	0.8 ± 0.1 ps
$t_{\text{max}, 2.0\text{eV}}$	~ 80 fs	~ 150 fs	~ 400 fs	~ 160 fs	~ 190 fs
$t_{\text{max}, 3.1\text{eV}}$	~ 70 fs	~ 190 fs	~ 160 fs	~ 300 fs	~ 170 fs

TABLE I. Fit parameters for single-exponential fits of pump-probe traces shown in Fig. 2.

	WS ₂ VB position	E_{gap}	$\Delta E_{\text{charge}}^{\text{WS}_2}$	$\Delta E_{\text{charge}}^{\text{Gr}}$
$\tau_{2.0\text{eV}}$	1.5 ± 0.2 ps	0.4 ± 0.2 ps	2.7 ± 0.9 ps	0.6 ± 0.1 ps
Amplitude _{2.0eV}	137 ± 6 meV	80 ± 30 meV	110 ± 10 meV	70 ± 10 meV
$\tau_{3.1\text{eV}}$	1.3 ± 0.1 ps	1.2 ± 0.2 ps	1.5 ± 0.2 ps	1.3 ± 0.1 ps
Amplitude _{3.1eV}	169 ± 8 meV	104 ± 8 meV	127 ± 6 meV	82 ± 3 meV
$t_{\text{max}, 2.0\text{eV}}$	~ 350 fs	~ 330 fs	~ 540 fs	~ 350 fs
$t_{\text{max}, 3.1\text{eV}}$	~ 400 fs	~ 410 fs	~ 200 fs	~ 190 fs

TABLE II. Fit parameters for single-exponential fits of pump-probe traces shown in Fig. 3.